IEEE Access
Multidisciplinary | Rapid Review | Open Access Journal

Received October 30, 2018, accepted November 18, 2018, date of publication December 6, 2018,
date of current version January 7, 2019.

Digital Object Identifier 10.1109/ACCESS.2018.2885381

Deployable Linear-to-Circular Polarizer Using PDMS Based on Unloaded and Loaded Circular FSS Arrays for Pico-Satellites

HIDAYATH MIRZA[1,2], TOUFIQ MD HOSSAIN[1], PING JACK SOH[1,3], (Senior Member, IEEE), MOHD FAIZAL JAMLOS[1,4], (Senior Member, IEEE), MUHAMMAD NAZRIN RAMLI[1], AZREMI ABDULLAH AL-HADI[1], (Senior Member, IEEE), EMAD S. HASSAN[2,5], AND SEN YAN[3,6], (Member, IEEE)

[1]Advanced Communication Engineering Centre, CoE, School of Computer and Communication Engineering, Universiti Malaysia Perlis, Pauh Putra Campus, Arau 02600, Malaysia
[2]Department of Electrical Engineering, College of Engineering, Jazan University, Jizan 45142, Saudi Arabia
[3]ESAT-TELEMIC Research Division, KU Leuven, 3001 Leuven, Belgium
[4]Faculty of Mechanical Engineering, Universiti Malaysia Pahang, Pekan 26600, Malaysia
[5]Department of Electronics and Electrical Communications, Faculty of Electronic Engineering, Menoufia University, Minuf 32952, Egypt
[6]School of Electronics and Information Engineering, Xi'an Jiaotong University, Xi'an 710049, China

Corresponding author: Ping Jack Soh (pjsoh@unimap.edu.my)

This work was supported in part by the Malaysian Ministry of Education via the Prototype Development Grant Scheme (PRGS) (grant no: PRGS/2/2015/ICT06/UNIMAP/02/1), in part by the Collaborative Research in Engineering, Science and Technology (CREST) R&D Grant (grant no: P12C2-17), in part by the UniMAP Special Endowment Fund (grant no: 7015-00004), and in part by the Research Foundation Flanders (F.W.O.) Postdoctoral Fellowship (grant no: 12O1217N).

ABSTRACT In this paper, flexible and deployable double-sided linear-to-circular polarizers designed on polydimethylsiloxane are proposed for the first time to the best of our knowledge. ShieldIt textile is used as the conducting element of the two designs based on two different unit cell arrays: a loaded circular patch unit cell or an unloaded circular patch unit cell, both backed by a generic rectangular element on its reverse side. This is in contrast to conventional frequency-selective structure-based linear-to-circular polarizers implemented using rigid substrates, which are multi-layered and requires inter-layer physical spacing. This complicates their implementation using flexible substrates and in a deployable format. Upon implementation of this double-sided polarizer, their final performances are evaluated in terms of the phase difference, conversion efficiency, 3-dB axial ratio (AR), and ellipticity bandwidth (from 40° to 45°). Measurements indicated good agreements with simulations, and both structures exhibited more than 90% of conversion efficiency from 2.34 to 3 GHz (for the loaded circular unit cell) and from 2.36 to 3 GHz (for the unloaded circular unit cell). In terms of ellipticity, a bandwidth of 8.67% is observed for the unloaded design and 13.82% for the loaded design. The unloaded structure exhibited a fractional 3-dB AR bandwidth of 36.36% (from 1.98 to 2.86 GHz) in simulations, and 32.64 % (from 2.00 to 2.78 GHz) when evaluated experimentally. Conversely, the loaded design showed only 12.58%. An equivalent circuit model is proposed and validated via a comparison between the circuit and full-wave simulations. Finally, the performances of these polarizers are also assessed under different bending conditions due to the use of flexible materials, prior to the proposal of a suitable deployment mechanism.

INDEX TERMS Flexible polarizer, linear-to-circular polarization, pico-satellite.

I. INTRODUCTION

In recent years, conventional satellites are increasingly being replaced by a constellation of low-cost and compact-sized pico-satellites [1]. This enables cost-effectiveness and specialized functions such as imaging, sensing, and deep space research. A type of such pico-satellites is known as Cube Satellites (CubeSats) [2], [3], which are usually deployed in or in some cases, beyond the Low Earth Orbit (LEO). The frequency spectrum for CubeSats has been recently regulated by the Federal Communications Commission (FCC). One of these recommended bands is the S-band, specified between 2.39 GHz and 2.45 GHz [4]. To ensure

reliability of communication, many types of high gain circularly polarized (CP) antenna topologies have been studied for its use, including conventional arrays and reflectarrays, reflector antennas, horns, multifeed and gain-enhanced microstrip antennas, etc [1]. However, these antennas require stringent design specifications, besides being conventionally implemented using rigid structures, which are difficult to integrate in CubeSats given their space constraint [9]. Moreover, due to the sizes of CubeSat (with the smallest of 1U size, equivalent to $10 \times 10 \times 10$ cm^3), antennas in deployable formats is almost an essential need for CubeSats, as they communicate in the UHF and S-band, which results in electrically large antennas and polarizers. This is evident from the current antennas used in CubeSats, which include deployable monopoles or dipoles. The use of linear-to-circular polarizer surfaces integrated with Linearly Polarized (LP) antennas has been reported as a versatile alternative approach in achieving broadband CP characteristics [1], [7]–[11]. The choice of linear-to-circular polarizers for CubeSats meets the necessary CP signal requirements, which minimizes noise, multipath interference, Faraday rotation, and propagation hindrance in rain [14]–[17]. Different linear-to-circular polarizers which are designed using FSS in different forms have been reported in literatures and presented in multi-layered substrate topologies with large inter-layer gaps [11], [12], [18]. Due to these reasons, their implementation in a compact or deployable format on pico-satellites becomes more complex. Moreover, the rigidity of the substrate causes hindrance to the integration of deployment mechanism as well. A brief comparison of the reported polarizers is tabulated in Table 1. It can be seen that most of the polarizers are designed on rigid surfaces, except our previous works in [9] and [10]. The CP characteristics of polarizers are assessed using the bandwidth $BW_{\eta_{conv}}$ with conversion efficiency η_{conv} higher than 90% [19]. At the same time, only the bandwidth, $BW_{3\ dB}$ exhibiting less than 3 dB of axial ratio (AR) is considered as operational [7]. Besides that,

TABLE 1. Comparison of recent linear-to-circular polarizers in terms number of layers and operating band.

Ref.	Substrate	Type	Band	$BW_{3\ dB}$	No. of layers
[5]	Rogers RT/Duroid 5870	Rigid	Ku	4.3%	1
[6]	Rogers RT/Duroid 5880	Rigid	Ka	34.9%	4
[7]	Rogers 5870	Rigid	K	5.6%	1
[8]	Rogers RT/Duroid 5880	Rigid	K	20%	3
[9]	Felt	Flexible	S	5.39%	1
[10]	Felt	Flexible	S	N/A	1
[11]	Arlon	Rigid	S-band and X-band	52%	2
[12]	ArlonDiclad 880	Rigid	X	N/A	4
[13]	FR-4	Rigid	X	66.7%	1
This work	PDMS	Flexible	S	32.64%	1

the ellipticity is also used to determine the shape of the polarization ellipse in this work. The bandwidth of the polarizers with at least 90 % of conversion efficiency ($BW_{\eta_{conv}}$) reported in [20] and [19] is 33% and 63%, respectively. However, these designs are fabricated using rigid materials, thus making it unsuited for deployable structures. In terms of axial ratio, the work in [7] featured a BW_{3dB} of 5.6 % and 4.3 % in first and second band, respectively. Nonetheless, the highest BW_{3dB} of 66.7 % has been reported in [13]. However, these designs are not flexible. On the other hand, the previous research utilizing flexible materials presented in [9] featured a limited BW_{3dB} bandwidth of 5.39 %.

This work presents the designs of two flexible linear-to-circular polarizers inspired by Munk [21]. These linear-to-circular polarizers are designed based on two types of unit cell designs, namely: (a) loaded circles inscribed in a circle (denoted as Design 1); and (b) unloaded circles inscribed in a circle (denoted as Design 2). Both designs are implemented using flexible PDMS to enable its deployable form. The implementation of such linear-to-circular polarizers in this flexible format, to the best of our knowledge, is the first to be reported for pico-satellite applications in the S-band, besides the initial simulation work from [9] and [10]. To ensure performance robustness, the proposed linear-to-circular polarizers are assessed in terms of ellipticity bandwidth, BW_{η}, conversion efficiency η_{conv} within 90 % of the η_{conv} bandwidth, denoted by $BW_{\eta_{conv}}$, and axial ratio (AR). Upon completion of the parameters' assessments for both designs, it is found that the unloaded topology (Design 2) featured a higher operational bandwidth. This structure is chosen to be further analyzed, fabricated and measured. Besides in planar conditions, the linear-to-circular polarizers are then characterized via bending evaluations, prior to the proposal a potential deployment model. This paper is structured as follows.

The next section presents the important parameters for the polarizer and their calculation methods, before the presentation of the loaded and unloaded unit cell designs. Next, the performance assessment of the two polarizers is presented and discussed before the description of the stowage and deployment schemes.

II. THEORY AND OPERATION OF LINEAR-TO-CIRCULAR POLARIZERS

A linearly-polarized (LP) wave is first considered incident on the linear-to-circular polarizer, with its E-field inclined at 45° relative to the positive x-axis. The orthogonal components of the incident and transmitted E- field along the x and y-axes can be decomposed and expressed as E_x^i, E_y^i and E_x^t, E_y^t, respectively. It is assumed that the decomposed orthogonal components of the incident electric field namely E_x^i, E_y^i are equal in terms of magnitude and phase [12] (i.e. $\left|E_x^i\right| = \left|E_y^i\right| = |E_0|$ and $\Phi_{E_x^i} = \Phi_{E_y^i}$). In such case, the unity value of q in (1), along with the phase characteristics in (2) will ensure circularly polarized (CP) wave to be

transmitted form the linear-to-circular polarizer [5], [6], [12], [13].

$$q = \frac{\left|E_x^t\right|}{\left|E_y^t\right|} = \frac{\left|E_x^i\right||T_x|}{\left|E_y^i\right||T_y|} \tag{1}$$

$$\left[\Phi_{E_x^i} + \Phi_{T_x}\right] - \left[\Phi_{E_y^i} + \Phi_{T_y}\right] = \pm n\frac{\pi}{2} \tag{2}$$

where T_x and T_y are the transmission coefficients for E_x^i and E_y^i respectively [10]. The value of q=1 and the criteria of the equal magnitude and phase of E_x^i and E_y^i reduce (1) and (2) into(3) and (4) [5]:

$$|T_x| = |T_y| \tag{3}$$

$$\Phi_{T_x} - \Phi_{T_y} = 2n\pi \pm n\frac{\pi}{2} \tag{4}$$

Besides that, other performance assessment parameters of linear-to-circular polarizer such as conversion efficiency (η_{conv}) and ellipticity (η) are used in [5], [13], and [19]. If the circular conversion coefficient for the right hand circularly polarized (RHCP) waves, C_-, and left hand circularly polarized (LHCP) waves, C_+, are expressed using (7) and (8), then η_{conv} and η are provided by (9) and (10) [5], [10], [12], [13], [19], [22], [23];

$$C_+ = E_x^i T_x - jE_y^i T_y \tag{5}$$

$$C_- = E_x^i T_x + jE_y^i T_y \tag{6}$$

$$\eta_{conv} = \frac{|C_-|^2 - |C_+|^2}{|C_-|^2 + |C_+|^2} \times 100 \tag{7}$$

$$\eta = \tan^{-1}\left(\frac{|C_+| - |C_-|}{|C_+| + |C_-|}\right) \tag{8}$$

A value of 45° ellipticity, η, represents the CP wave and a 0° value indicates LP wave [13], [24].

III. PRINCIPLE OF OPERATION AND DESIGN METHODOLOGY

A. PRINCIPLE OF OPERATION AND DESIGN

As briefly explained in the introduction, two designs of the flexible PDMS-based transmission type linear-to-circular polarizers are investigated in this work. The design is based on the gap or slot structures which primarily contribute to additional capacitive effects, whereas the planar conductive structures result primarily in additional inductance to the transmitted electric field. The goal is to achieve phase advanced and phase retarded characteristics for the two orthogonal components of transmitted electric field, namely E_x^t and E_y^t. Due to the inherent characteristics of the inductive and capacitive structures, phase differences can be introduced between the orthogonal components of the transmitted electric field E_x^t and E_y^t. Both structures are designed based on the procedure proposed in [21]. Their topologies are illustrated in Fig. 1, while their dimensions are summarized in Table 2. PDMS substrate with a height of 3 mm and relative permittivity (ε_r) of 2.7 is used for both designs. To ensure a fair comparison, the same ShieldIt conductive textile (with an estimated conductivity of 1.18×10^5 S/m and 0.17 mm of thickness) is used in both designs as their conducting elements. Besides that, all polarizers are designed and optimized using a standard commercial electromagnetic solver, CST Microwave Studio. Simulations were performed using the Floquet port using the unit cell boundaries, whereas in practice, a 4 × 4 array of the proposed unit cells is used to form the polarizer.

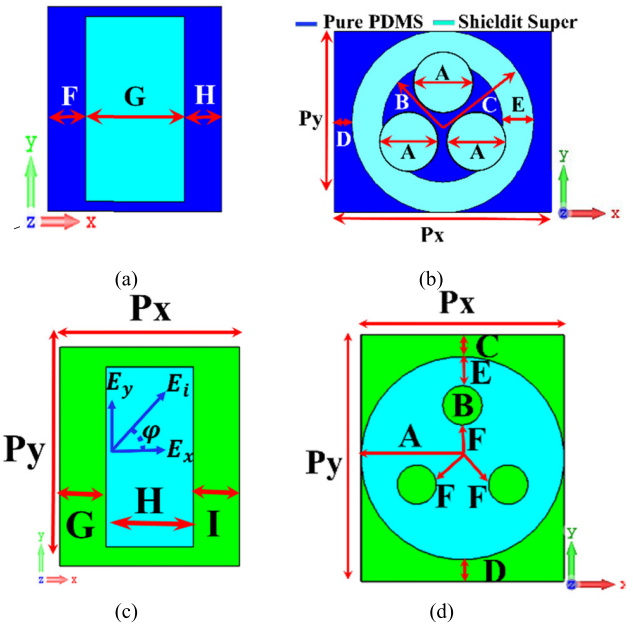

FIGURE 1. Topology of Design 1 (loaded) (a) front view; and (b) back view; and Design 2 (unloaded) (c) front view (d) back view.

TABLE 2. Dimensions (in mm) of the proposed designs.

Param.	Design 1	Design 2	Param.	Design 1	Design 2
A	10	23	G	41	11.7
B	20	9	H	15.5	22.5
C	30	5	I	N/A	11.7
D	5.8	5	Px	72	46
E	5.8	6.5	Py	60	56.2
F	15.5	7.5			

The unit cell for Design 1 is a circular outer ring consisting of three circles inscribed inside this outer ring. The centers of these three circles are situated in the vertex of a virtual equilateral triangle. The unit cells in Design 1 are physically connected in the y-direction, which contributes to higher inductance for the y-polarized component (E_y^t). Meanwhile, the unit cell for Design 2 consists of a circular patch integrated with three circular slots to provide extra capacitance in the y-polarized component of transmitted electric field (i.e., E_y^t).

The circular slots are arranged similarly as the previous design within the circular patch. Furthermore, the unit cells are connected with each other in x-direction (contrary to Design 1, where they are connected in y-direction) to incorporate higher inductance value for the x-polarized

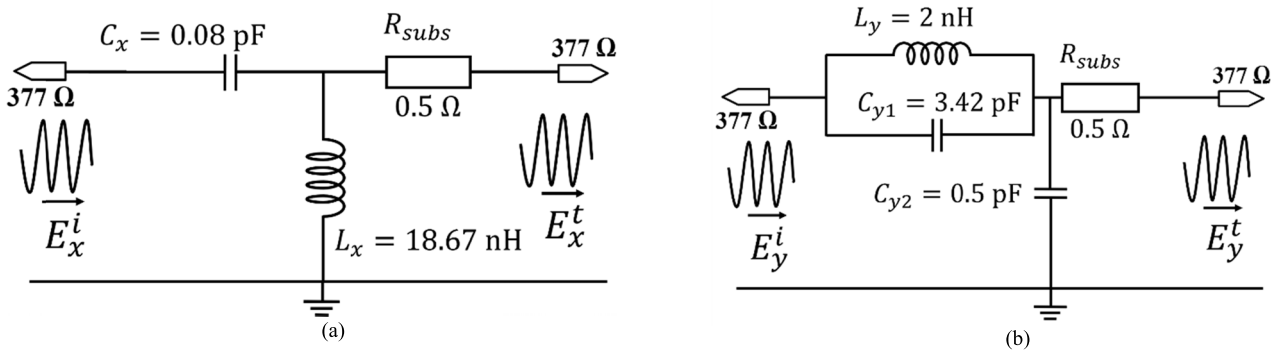

FIGURE 2. Equivalent circuit model for (a) x-polarized and, (b) y-polarized Electric field.

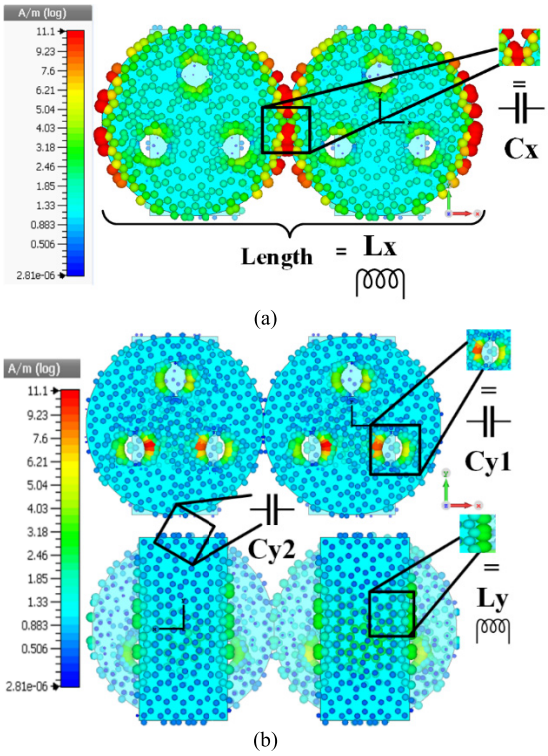

FIGURE 3. Surface current for (a) x-polarized and, (b) y-polarized Electric field.

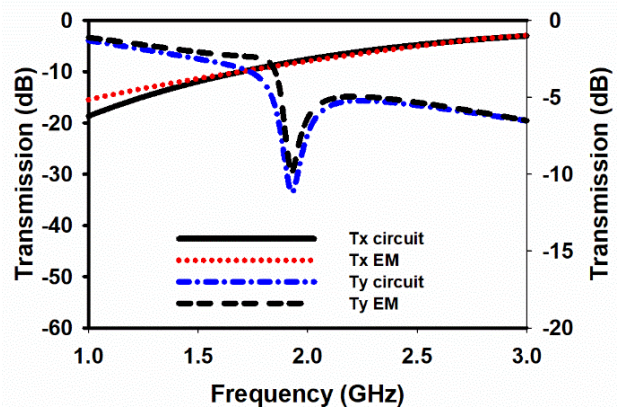

FIGURE 4. Comparison of Transmission coefficient results of full wave EM simulation of CST and circuit simulation of Fig. 2.

component (E_x^t). Conversely, the unit cells for Design 2 are kept separated from each other in y-direction to increase capacitance in this direction. The radius of the loaded circles (for Design 1) and slots (for Design 2) are optimized to obtain the circular polarization characteristics based on the requirements in equations (1) to (4). Moreover, to enable a higher degree of freedom during optimization of the polarizer's performance, a rectangular patch parallel to the y-axis is introduced in front of both structures, resulting in an inductive effect for E_y^t.

B. EQUIVALENT CIRCUIT MODEL

Due to favorable characteristics of Design 2 (the unloaded structure), this design is to be studied further before its fabrication and further discussion. This study includes the modeling of its equivalent circuit model, as illustrated in Fig. 2. It can be seen from this figure that the inductance in x- polarized condition, L_x, has a higher value of 18.67 nH relative to that of the y-polarized condition, L_y (2 nH). On the other hand, the opposite electrical characteristics is observed in the x-polarization condition, as can be seen in the reduced capacitance values of C_x compared to C_{y1}. The former, C_x, with smaller surface area, is located within the limited space near to the connecting junction between two consecutive unit cells, as shown in the surface currents illustrated in Fig. 3(a). The surface current characteristics provided insight to the design principle of the polarizer in both polarizations as follows. In the x-polarization, the circular slots remained not excited. On the other hand, in the y-polarization (Fig. 3(b)), the slots are excited, which gives rise to higher capacitance value of C_{y1}, with a small capacitance value (C_{y2}) formed in the front plane between two excited metal strips.

IV. PERFORMANCE ASSESSMENT OF POLARIZERS

A. DEPLOYED CONDITION

In general, it is observed that the all prototypes are operational within the S-band frequency from 2.39 to 2.45 GHz, as specified by FCC. The linear-to-circular polarizer of Design 2 has

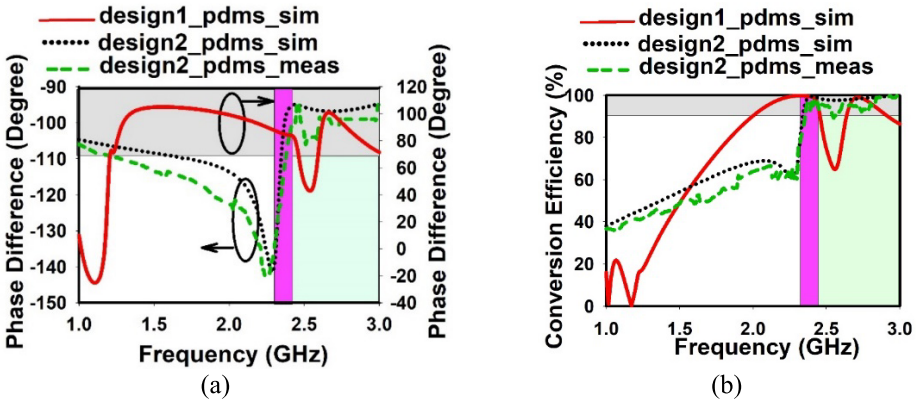

FIGURE 5. Simulated and measured results of proposed linear-to-circular polarizer in flat (deployed) condition: (a) Phase Difference, $\Delta\Phi = \Phi_{Tx} - \Phi_{Ty}$ (b) Conversion efficiency.

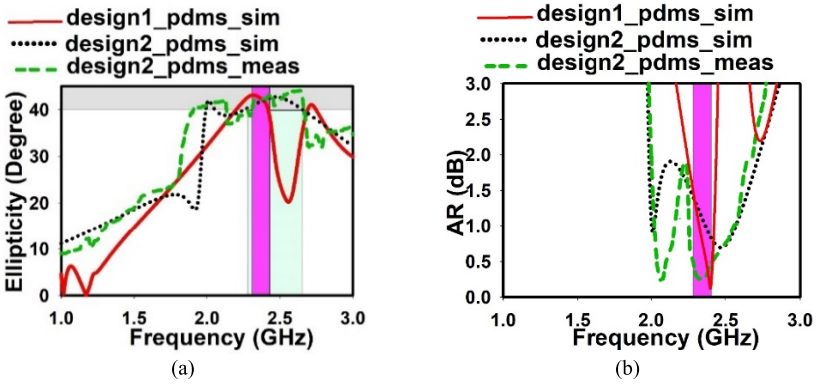

FIGURE 6. (a) Ellipticity and (b) Axial Ratio of the proposed designs in flat (deployed) condition.

TABLE 3. Summary of the performance of proposed polarizers when assessed in a flat (deployed) condition.

Design	Substrate	Frequency band (GHz)					$\lvert T_x\rvert = \lvert T_y\rvert$			
		η_{conv} >90%	η=40fl - 45° ellipticity	Phase Diff. (90 °± 10°)	AR<3 dB	Operational bandwidth	Freq. (GHz)	$\Delta\Phi$ (°)	η_{conv}	η (°)
Design 1	Simulated	1.99-2.46	2.21-2.41	1.99-2.45	2.16-2.45 & 2.66-2.84	2.21-2.41	2.35	85.41	99.67	32.61
Design 2	Simulated	2.34-3.00	2.26-2.65	2.34-3.00	1.98-2.86	2.34-2.65	2.43	-94.87	99.64	42.57
	Measured	2.36-3.00	2.31-2.66	2.38-3.00	2.00-2.78	2.38-2.66	2.41	-100	95.44	39.30

outperformed Design 1 in terms of bandwidth in general, particularly where $|T_x| = |T_y|$. Due to the favorable behavior of Design 2 in terms of conversion coefficient and ellipticity, this structure has been chosen to be fabricated and assessed experimentally. During these experimental assessments, the fabricated polarizer is placed between two standard gain horns (A-INFOMW LB-8180) and was measured using an Agilent E5170C ENA network analyzer. Fig. 4 and 5(a) illustrates the magnitude and phase difference of T_x and T_y, respectively. Meanwhile, Fig. 5(b), Fig. 6(a) and Fig. 6(b) represents the conversion efficiency, ellipticity and axial ratio, respectively. The (purple) shaded zone represents the allocated pico-satellite spectrum by FCC (i.e. 2.39 GHz to 2.45 GHz), whereas the frequency range with $90° \pm 10°$ phase difference, frequency range with conversion efficiency, $\eta_{conv} \geq 90$ %, and frequency range with ellipticity η of a value between 40° to 45° are also shaded (in silver) for clarity in Figs. 5, 6 and 7. The performance of the proposed designs in their deployed condition is summarized in Table 3. To provide further insight of the results, an "operational bandwidth" is presented in Table 3, which represents the band in which all four criteria of linear-to-circular polarizers (viz. $\eta_{conv} >$ 90%, η variation between 40° and 45°, $\Delta\Phi = (90° \pm 10°)$ and AR < 3 dB) are fulfilled. In general, it can be seen that the

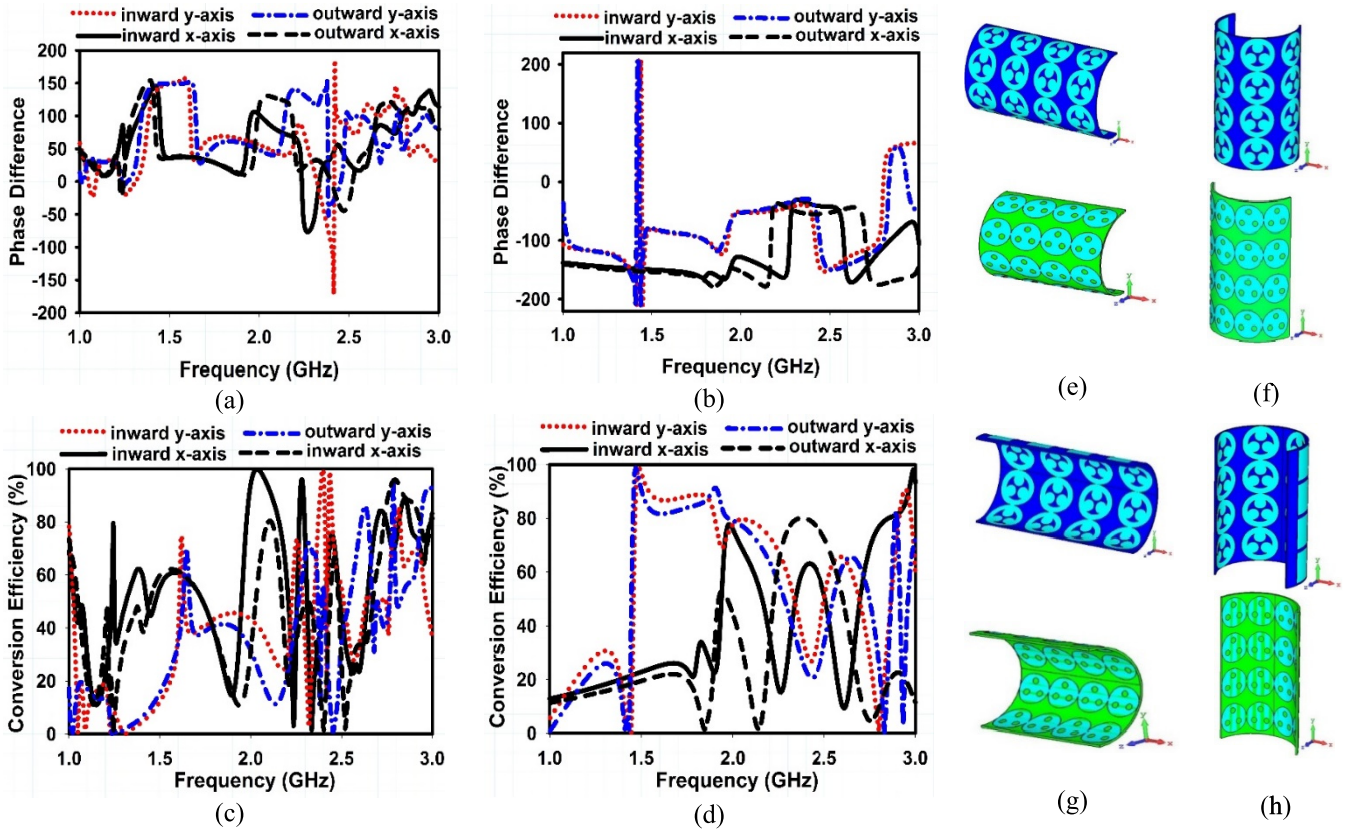

FIGURE 7. Different characteristics of the linear-to-circular polarizer under bending condition. Phase characteristics: (a) loaded, (b) unloaded Conversion efficiency: (c) loaded (d) unloaded. 3D bending geometry in bending condition :(e) around z axis towards +x-axis, (f) y-axis bending; outwards bending (g) x-axis, (h) y-axis.

unloaded linear-to-circular polarizer from Design 2 exhibited a greater fractional operating band than the loaded linear-to-circular polarizer from Design 1. In terms of conversion efficiency, $\eta_{conv} > 90$ %, Design 1 showed a fractional bandwidth of 21.12 % (from 1.99 to 2.46 GHz). On the other hand, measurements for Design 2 indicated a fractional bandwidth of 23.88 % (from 2.36 GHz to 3 GHz) with $\eta_{conv} \geq 90$ %, which is slightly lower than the 24.72 % bandwidth shown in simulations. However, for the criteria of $\eta = 40°$-$45°$, the measured fractional bandwidth is 14.08 % (from 2.31 GHz to 2.66 GHz), compared to a 13.82 % fractional bandwidth in simulations.

Conversely, the performance of Design 1 is poorer in this aspect, with a limited value of 8.67 %. For Design 1, the $90° \pm 10°$ phase difference criteria is fulfilled with a fractional bandwidth of 20.72 %. In contrast, the fractional bandwidth of 23.05 % is shown by the unloaded linear-to-circular polarizer of Design 2 in measurements, whereas 24.72 % of bandwidth is obtained in simulations. In terms of axial ratio performance, Design 2 has outperformed Design 1 by exhibiting BW_{3dB} (fractional bandwidth with < 3 dB of axial ratio) of 36.36 % (from 1.98 GHz to 2.86 GHz) in simulations and 32.64 % (from 2.00 GHz to 2.78 GHz) in measurements. Finally, measurements within the band based on $|T_x| = |T_y|$ also agree well with simulations. A more general conclusion can be drawn by assessing the operational bandwidth of each design (shown in Table 3). For the loaded linear-to-circular polarizer structure (Design 1), the operational bandwidth $BW_{operation}$ is only 10.94 %. Meanwhile, the unloaded structure shows a $BW_{operation}$ value of 11.11 % in measurements, in comparison to 12.42 % obtained from simulations.

B. ASSESSMENT IN BENT CONDITION AND DEPLOYMENT PROCESS

Due to the flexible substrates used and the proposed implementation in a deployable format, the linear-to-circular polarizers are studied further under bent conditions to predict their performance under imperfect deployment. The deployment process includes three main stages: (i) stowage, (ii) boom deployment, and (iii) full polarizer deployment, as discussed in [10]. The use of polarizer in combination with linearly polarized antenna is a rather challenging new concept for pico-satellites, and can only be realized once both elements can be compact, lightweight and flexible. The difference between previously proposed foldable structure in [10] is that the present work is deployable from a rolled form. To perform assessments under bent conditions, the polarizer is bent over a hypothetical vacuum cylinder in the simulator. The radius of

TABLE 4. Summary of the polarizer performance operating under bending conditions.

Prototype	Parameter	Frequency (GHz)	Condition of polarizer				
			Flat (deployed)	Bent inwards at *x*-axis	Bent inwards at *y*-axis	Bent outwards at *x*-axis	Bent outwards at *y*-axis
Design 1	Phase diff (°)	2.39	84.44	33.41	-81.33	6.84	-36.16
		2.45	76.62	53.00	90.90	-38.39	-4.23
	Conv. eff (%)	2.39	99.40	40.35	96.36	10.23	40.52
		2.45	92.66	75.40	80.08	62.03	2.19
Design2	Phase diff (°)	2.39	95.48	-38.09	-49.72	-54.76	-30.94
		2.45	94.58	-41.65	-149.95	-54.49	-115.09
	Conv. eff (%)	2.39	99.49	61.63	32.70	80.05	24.88
		2.45	99.67	61.51	30.10	77.56	21.42

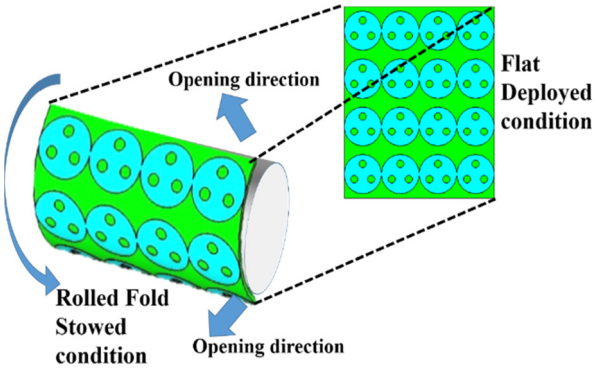

FIGURE 8. Stowed and deployed state of the polarizer.

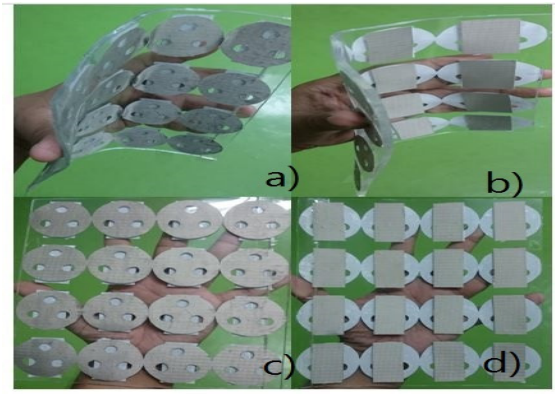

FIGURE 9. Fabricated unloaded PDMS polarizer in bent (top) and flat condition (bottom): (a),(c) Rear view (b),(d) Front view.

this cylinder is 70 mm, and the proposed linear-to-circular polarizer is bent around it at the *x*- and *y*-axes. The bent conditions are assessed at two frequencies: 2.39 GHz and 2.45 GHz, and their performance is summarized in Table 4. Design 2 is found to offer more conversion efficiency when bent at the *x*-axis. This can be explained from the concept described in Section III. When the wave is traveling outwards from the linear-to-circular polarizer (in the *z*-direction) they are not much affected due to the limited bending in the *x*-axis. The connection between circular slots, which are the main contributing component to the operation of this structure are minimally affected in such bending scenario. However, for Design 1, in general, the *y*-axis bending has shown better performance compared to its *x*-axis bending. This is due to the rectangular metal strip located in the forward plane of the unit cell, parallel to the *y*-axis. For the case of the *x*-axis bending, more area of this strip is bent, resulting in performance degradation of the polarizer. On the contrary, a smaller area of this metal strip is bent with the *y*-axis bending, resulting in a better performance. Design 2 is fabricated, as shown in Fig. 9. This structure based on Design 2 can be stowed with an *x*-axis bending (whether inwards or outwards) prior to full deployment on the pico-satellites.

V. CONCLUSION

Two designs of flexible and deployable linear-to-circular polarizers for pico-satellites are proposed and studied in this work. PDMS is used for the first time as their substrate, whereas their conductive elements are formed using commercial conductive textile, ShieldIt Super. Two unit cell designs, a rectangular-shaped patch backed by loaded circular patches (Design 1) and unloaded circular slots (Design 2) were first evaluated numerically. Measurements indicated good agreements with simulations, and both structures exhibited more than 90 % of conversion efficiency from 2.34 to 3 GHz (for the loaded circular unit cell) and from 2.36 to 3 GHz (for the unloaded circular unit cell). In terms of ellipticity, a bandwidth of 8.67 % is observed for the unloaded design and 13.82 % for the loaded design. The unloaded structure exhibited a fractional 3dB AR bandwidth of 36.36 % (from 1.98 GHz to 2.86 GHz) in simulations, and 32.64 % (from 2.00 GHz to 2.78 GHz) when evaluated experimentally. Conversely, the loaded design showed only 12.58 %. An equivalent circuit model is proposed and its operation is explained based on the surface current analysis. To validate this model, it is simulated using a circuit simulator and its performance is compared with results from the full wave solver. Assessment of the polarizers under bending conditions are also performed as a pre-implementation validation for the proposed rolled and foldable deployment scheme. All polarizers exhibited acceptable performance for use in the S-band frequencies for CubeSat. The fabricated design using PDMS also featured a large operating bandwidth, and good agreements between simulations and measurements.

ACKNOWLEDGMENT

The technical contributions of Dr. Rizwan Khan Jadoon is acknowledged.

REFERENCES

[1] A. H. Lokman *et al.*, "A review of antennas for picosatellite applications," *Int. J. Antennas Propag.*, vol. 2017, Apr. 2017, Art. no. 4940656.

[2] C. J. Vourch and T. D. Drysdale, "Inter-CubeSat communication with V-band 'bull's eye' antenna," in *Proc. Eur. Conf. Antennas Propag. (EuCAP)*, Apr. 2014, pp. 3545–3549.

[3] N. Chahat, J. Sauder, R. E. Hodges, M. Thomson, and Y. Rahmat-Samii, "The deep-space network telecommunication CubeSat antenna: Using the deployable Ka-band mesh reflector antenna," *IEEE Antennas Propag. Mag.*, vol. 59, no. 2, pp. 31–38, Apr. 2017.

[4] "Guidance on obtaining licenses for small satellites," Federal Commun. Commission, Washington, DC, USA, FCC Public Notice, Tech. Rep. DA-13-445, 2013, p. 5.

[5] I. Sohail, Y. Ranga, K. P. Esselle, and S. G. Hay, "A linear to circular polarization converter based on Jerusalem-Cross frequency selective surface," in *Proc. 7th Eur. Conf. Antennas Propag.*, Apr. 2013, pp. 2141–2143.

[6] L. Martinez-Lopez, J. Rodriguez-Cuevas, J. I. Martinez-Lopez, and A. E. Martynyuk, "A multilayer circular polarizer based on bisected split-ring frequency selective surfaces," *IEEE Antennas Wireless Propag. Lett.*, vol. 13, pp. 153–156, 2014.

[7] Y. Ranga, L. Matekovits, S. G. Hay, and T. S. Bird, "An anisotropic impedance surface for dual-band linear-to-circular transmission polarization convertor," in *Proc. Int. Work. Antenna Technol. (iWAT)*, no. 1, Mar. 2013, pp. 47–50.

[8] M. Hosseini and S. V. Hum, "A circuit-driven design methodology for a circular polarizer based on modified Jerusalem cross grids," *IEEE Trans. Antennas Propag.*, vol. 65, no. 10, pp. 5322–5331, Oct. 2017.

[9] H. Mirza *et al.*, "Single layered swastika-shaped flexible linear-to-circular polarizer using textiles for S-band application," *Int. J. RF Microw. Comput.-Aided Eng.*, vol. 28, no. 7, p. e21463, 2018.

[10] H. Mirza *et al.*, "A crossed dodecagonal deployable polarizer on textile and polydimethylsiloxane (PDMS) substrates," *Appl. Phys. A, Solids Surf.*, vol. 124, no. 2, p. 178, 2018.

[11] M. Fartookzadeh and S. H. M. Armaki, "Dual-band reflection-type circular polarizers based on anisotropic impedance surfaces," *IEEE Trans. Antennas Propag.*, vol. 64, no. 2, pp. 826–830, Feb. 2016.

[12] W. Zhang, J.-Y. Li, and L. Wang, "Broadband circular polarizer based on multilayer gradual frequency selective surfaces," *Int. J. Antennas Propag.*, vol. 2016, Aug. 2016, Art. no. 4928109.

[13] S. Yan and G. A. E. Vandenbosch, "Compact circular polarizer based on chiral twisted double split-ring resonator," *Appl. Phys. Lett.*, vol. 102, no. 10, p. 103503, 2013.

[14] M. Euler, V. Fusco, R. Dickie, R. Cahill, and J. Verheggen, "Sub-mm wet etched linear to circular polarization FSS based polarization converters," *IEEE Trans. Antennas Propag.*, vol. 59, no. 8, pp. 3103–3106, Aug. 2011.

[15] J. C. Batchelor and R. J. Langley, "Microstrip annular ring slot antennas for mobile applications," *Electron. Lett.*, vol. 32, no. 18, p. 1635, Aug. 1996.

[16] X. Ma, C. Huang, M. Pu, C. Hu, Q. Feng, and X. Luo, "Single-layer circular polarizer using metamaterial and its application in antenna," *Microw. Opt. Technol. Lett.*, vol. 54, no. 7, pp. 1770–1774, 2012.

[17] R. E. Hodges, D. J. Hoppe, M. J. Radway, and N. E. Chahat, "Novel deployable reflectarray antennas for CubeSat communications," in *IEEE MTT-S Int. Microw. Symp. Dig.*, May 2015, pp. 1–4.

[18] H. Zhu, K. L. Chung, X. L. Sun, S. W. Cheung, and T. I. Yuk, "CP metasurfaced antennas excited by LP sources," in *Proc. IEEE Antennas Propag. Soc. AP-S Int. Symp.*, vol. 1, Jul. 2018, pp. 1–2.

[19] J. Wang, Z. Shen, W. Wu, and K. Feng, "Wideband circular polarizer based on dielectric gratings with periodic parallel strips," *Opt. Express*, vol. 23, no. 10, pp. 12533–12543, 2015.

[20] M. Mutlu, A. E. Akosman, G. Kurt, M. Gokkavas, and E. Ozbay, "Experimental realization of a high-contrast grating based broadband quarter-wave plate," *Opt. Express*, vol. 20, no. 25, pp. 27966–27973, 2012.

[21] B. A. Munk, *Frequency Selective Surfaces: Theory and Design*, vol. 29. Hoboken, NJ, USA: Wiley, 2000.

[22] M. Mutlu, A. E. Akosman, and E. Ozbay, "Broadband circular polarizer based on high-contrast gratings," *Opt. Lett.*, vol. 37, no. 11, pp. 2094–2096, 2012.

[23] H.-X. Xu, G.-M. Wang, M. Q. Qi, T. Cai, and T. J. Cui, "Compact dual-band circular polarizer using twisted Hilbert-shaped chiral metamaterial," *Opt. Express*, vol. 21, no. 21, pp. 24912–24921, 2013.

[24] J. Costantine, Y. Tawk, C. G. Christodoulou, I. Maqueda, M. Sakovsky, and S. Pellegrino, "A new UHF deployable antenna for CubeSats," in *Proc. IEEE Antennas Propag. Soc. AP-S Int. Symp.*, Jul. 2015, pp. 1426–1427.

Authors' photographs and biographies not available at the time of publication.